Oxidative Dehydrogenation Dimerization of Propylene over Bismuth Oxide: Kinetic and Mechanistic Studies

MARK G. WHITE,[1] AND JOE W. HIGHTOWER[2]

Department of Chemical Engineering, Rice University, Houston, Texas 77251

Classical kinetic experiments together with pulse microreactor studies involving deuterium and carbon-13-labeled isotopic tracers were used to investigate the oxidative dehydrogenation dimerization (OXDD) of propylene to 1,5-hexadiene and benzene over bismuth oxide between 748 and 898°K. The kinetic data, which indicated that the OXDD reaction is of variable order with respect to oxygen and propylene concentrations, could be fit to rate equations based on either the Langmuir–Hinshelwood model or the Mars–van Krevelen model, although the former gave more linear Arrhenius plots. A significant kinetic isotope effect ($k_H/k_D = 1.7$ at 873°K) shows that the rate-limiting step for the OXDD reaction involves C–H cleavage, and there is only a small amount of H/D scrambling among reactant and product molecules. Analysis of liquid products by infrared spectroscopy indicated that both 1,5-hexadiene and 1,3-cyclohexadiene are stable reaction intermediates; microreactor results involving unlabeled propylene, 1,5-hexadiene, 1,3-cyclohexadiene, and 1,4-cyclohexadiene as reactants confirmed the infrared findings. Pulse microreactor experiments with ^{13}C-labeled propylene clearly showed that deep oxidation (complete combustion) occurs via a consecutive-parallel network involving the partially oxidized intermediates as well as the starting propylene. Changes in the particle size do not alter the overall activity, although larger particles have lower selectivities for C_6 products than do smaller particles.

INTRODUCTION

Several studies of the catalytic oxidative dehydrogenation dimerization (OXDD) of propylene to 1,5-hexadiene have been reported in the patent literature (*1–4, 17*) and in journal articles (*5–16, 22–24*). These studies have been reviewed recently by Mamedov (*24*). Among the suitable catalysts for this reaction are tin(IV)–sodium oxide (*9, 15*), sodium–manganese oxide (*1, 2*), lead(II) oxide (*3*), cadmium oxide (*17*), thallium oxide (*17*), indium oxide (*8*), bismuth oxide (*4*), and bismuth–tin oxide (*16*). Reaction conditions for the OXDD of propylene over these catalysts are similar: temperatures 723–897°K, space times 0.1 to 1.0 sec, and propylene-to-oxygen partial pressure ratios of 1:1 to 6:1. Most of the catalysts for the OXDD reaction are low

surface area (0.1 to 1.0 m²/g) materials; internal pore diffusion has a deleterious effect on the selectivity to the dimer product 1,5-hexadiene.

There is general agreement that these reactions proceed through an oxidation/reduction cycle with the rate-limiting step being removal of an allyl hydrogen from the olefin followed by reactive coupling of the radicals. In the depletive mode (no gaseous O_2), a bismuth oxide "catalyst" becomes reduced to bismuth metal (*22*) and the reaction is first order in the propylene partial pressure. With O_2 present, the reaction over Bi_2O_3 is still first order in olefin and zero order in O_2 (*13*), and the selectivity to C_6 compounds is decreased.

These kinetics are different from those observed by Trimm and Doerr (*8*) who found that their data fit a multisite Langmuir–Hinshelwood model over an indium oxide catalyst. Similar conclusions were reached by Sciyama *et al.* (*25*) over bismuth–tin oxide. Other studies have led

to conflicting observations about the dependence on the oxygen partial pressure, some authors reporting first order (27) and others (26) reporting negative reaction orders.

One purpose of this work was to try to resolve some of these kinetic uncertainties by studying the rate dependence on the selected partial pressures under carefully controlled conditions. A second objective was to explore the origin of and interconversion among some of the minor products, such as the cyclohexadienes. Finally, deuterium-labeled tracers were used to identify rate-limiting steps and the scrambling of H and D atoms among the molecules.

EXPERIMENTAL

Reaction system. Classical kinetic experiments were conducted in a downflow plug flow reactor. The reactor was a 15-mm-i.d. Vycor tube 0.3-m long fitted with a centered 6-mm-o.d. Vycor thermowell in which the temperature could be measured at any point along the entire reactor length. Plugs of Vycor wool supported the catalyst and served as a preheater upstream of the bed. Helium, propylene, and oxygen were individually metered through needle valves with constant downstream pressure flow controllers, and the flow rates were measured by calibrated rotameters. Prior to entering the reactor, the gases were mixed in a tube filled with $\frac{1}{8}$-in. (3.2-mm) cylindrical pellets of Type 4-A Linde molecular sieves. Condensable liquids were allowed to separate from the product gases in a disengaging volume.

Chemicals. The catalyst was ultrapure Bi_2O_3 from Alpha Inorganics and had a surface area of 0.7 m^2/g. Zero grade helium from Liquid Carbonics, chemically pure grade propylene from Union Carbide (Linde Division), and extra dry oxygen (also from Linde) were used without further purification. Deuterium-labeled propylene (1,1,3,3,3-propylene-d_5, 98% enrichment) and [3-^{13}C]propylene (C=C-^{13}C, 56% enrichment) were obtained from Merck, Sharp, and Dohme. Calibration amounts of

the hexadienes (1,3-, 1,4-, and 1,5-) and cyclohexadienes (1,3- and 1,4-) came from Chem Samples.

Analytical. Gaseous products were analyzed with a 2-m, $\frac{1}{8}$ in. (3.2-mm) o.d. column of Poropak Q operated isothermally at 423°K in a Perkin–Elmer 3920 gas chromatograph. Liquid products were analyzed by a combination of GLC (6-m-long, 8-mm-o.d. column of Carbowax 20M on acid-washed Chromosorb W at 353°K), mass spectrometry, and infrared spectroscopy after being distilled into appropriate fractions. Mass spectral analyses were carried out on a CEC 21-104 instrument at low-ionization voltages to minimize fragmentation. The normal ^{13}C isotope and fragmentation corrections were applied to the parent peaks of the various molecules.

Reaction procedures. The reactor was operated in two different modes: one was in the steady state and the other was as an unsteady state microcatalytic pulse reactor. The total pressure in both operational modes was 1.54 atm (156.4 kPa). The reactor temperature, monitored potentiometrically with an iron constantan thermocouple, was controlled in the range of 748 to 989°K to within ±1°K with an L & N Electromax controller. In the steady-state mode oxygen was always the limiting reactant (the ratio He : propylene : O_2 was typically in the range 12 : 4 : 1); conversions x shown in the figures are based on oxygen utilization. Vapor-phase product samples were taken with an on-line heated valve and sampling loop connected directly to the GLC.

Helium carrier gas was also used in the pulse studies. 2.4 cm^3 (STP) pulses of various hydrocarbons were injected in the absence of gas phase oxygen via a dosing valve, and the reaction products were collected in a liquid nitrogen trap for subsequent analysis.

Sample weights of catalyst ranged from 2.5 to 15.6 g of Bi_2O_3 in various parts of these studies; the weights used are shown in captions for the figures. The space time τ, in units of gram-second per cubic meter,

is the catalyst weight in kilograms divided by the volumetric flow rate in cubic meters per second measured at reactor temperature and pressure. In these experiments the space time ranged from 0.5×10^3 to 30×10^3 kg-sec/m³.

Definition of selectivity. Since under some reaction conditions part of the 1,5-hexadiene (HD) product was dehydrocyclized to benzene (Bz), both of these C_6 species were lumped together in calculating the selectivity for the coupling reaction, viz.

$$\% \text{ Selectivity} = \frac{S}{(S + 1)} \times 100 \qquad (1)$$

where $S = 6(C_{HD} + C_{Bz})/C_{CO_2}$. The factor 6 in the selectivity ratio S accounts for the different number of carbon atoms in the C_6 and CO_2 products. Calculated in this manner, the selectivity is the moles of C_6 products divided by the total moles of propylene converted.

RESULTS

Kinetics, Steady-State Flow Reactor

Typical low conversion data from the steady state flow reactor at two different oxygen concentrations (constant excess propylene in diluent helium) are shown in Fig. 1. "Initial" differential reactions rates $(dz/d\tau)$ are calculated from such plots. Fractional conversion rate data obtained at different temperatures between 748 and 893°K are shown on a semilog plot vs. $1/T$
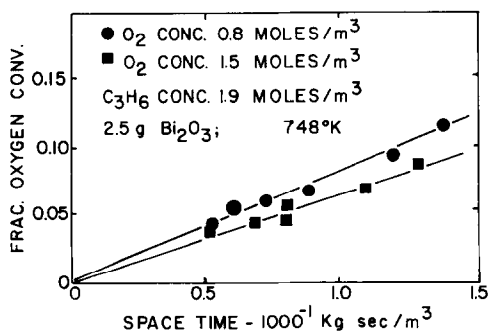

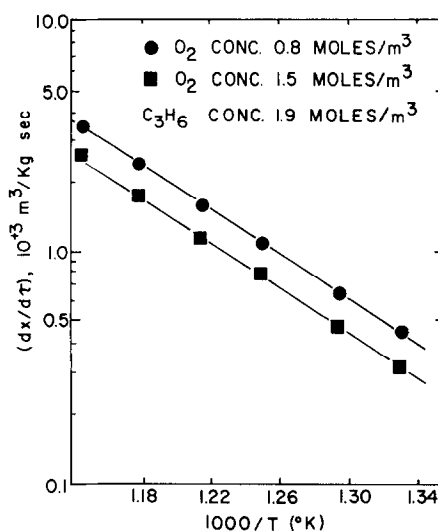FIG. 1. Oxygen conversion as a function of space time.

FIG. 2. Arrhenius plot for OXDD of propylene over Bi_2O_3.

in Fig. 2 to give an apparent Arrhenius activation energy; that value is 22.0 kcal/mole (92.1 KJ/mole).

Although the explosion limits of the gas mixtures restricted the range over which the concentrations could be varied, it was possible to change first one and then the other partial pressure of the reactants to obtain apparent reaction orders. The reaction is less than first order in oxygen, as shwon by the concave (with respect to the abscissa) curve in Fig. 3 when the initial isothermal rates (moles O_2/kg sec) are plotted versus oxygen concentration. However, the reaction is slightly greater than first order in propylene as indicated by the convex curvature of the rate vs. propylene concentration in Fig. 4.

The single curve in Fig. 5 clearly shows that the *oxygen consumption rate* is not affected by the particle size in the range 74 to 3360 μm. However, the *selectivity* is a function of particle size, as seen by the three separate curves in Fig. 6. Notice that the smallest particles give the highest selectivity.

External transport effects did not affect the rate, since varying the catalyst weight
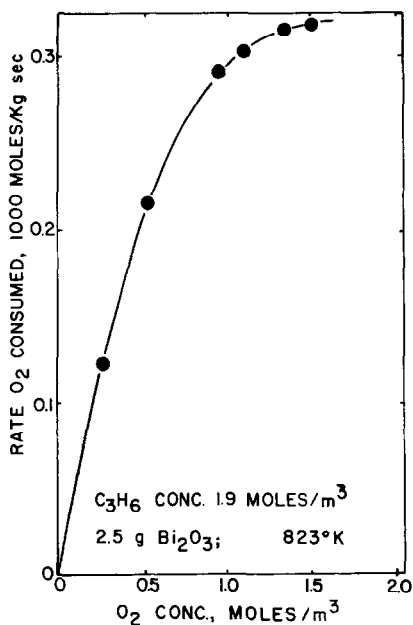
FIG. 3. Initial rates of oxygen consumption versus oxygen concentration.

at constant space time did not alter the fractional conversion.

Data at higher conversions were also collected and tested according to integrated rate equations shown in the Discussion section.
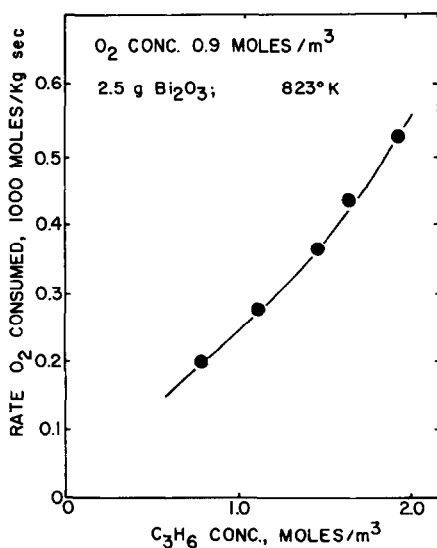

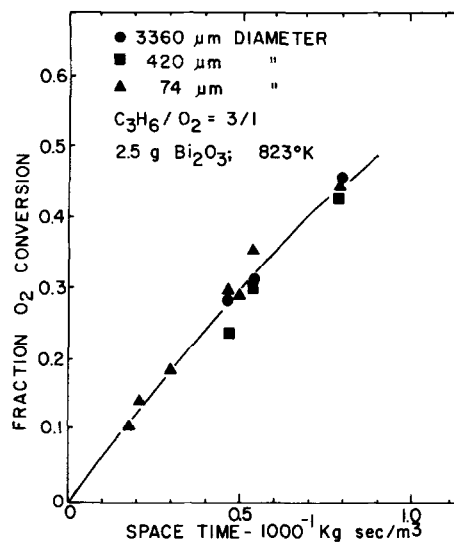FIG. 4. Initial rates of oxygen consumption versus propylene concentration.

FIG. 5. Particle size effects on activity.

Other Reaction Products

The primary reaction products were 1,5-hexadiene, benzene, CO_2, and of course water as shown by the GLC trace in Fig. 7. However, lesser amounts of 1,3-cyclohexadiene and 1,4-hexadiene were also formed. These observations were confirmed by infrared spectra of the condensed liquid products and by GLC.

It is possible that the hexadienes and cyclohexadienes may be intermediates along the pathways leading to benzene formation.
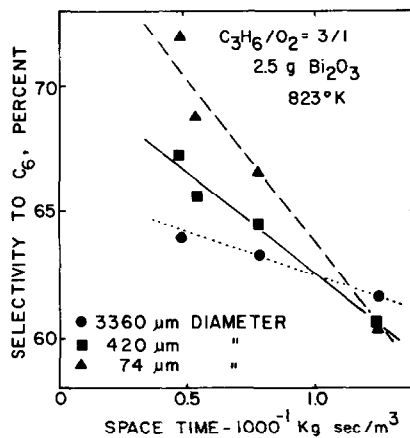

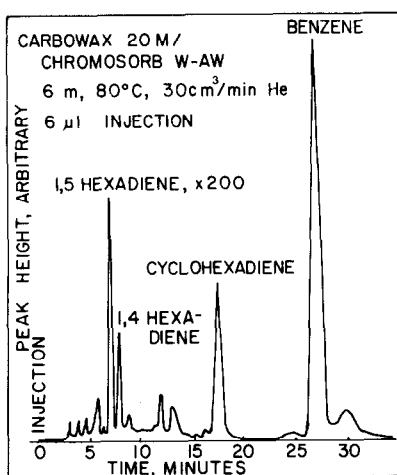FIG. 6. Particle size effects on selectivity.

FIG. 7. Chromatogram of liquid products.

To test their activities relative to that of propylene, 2.4 cm^3 (STP) pulses of various hydrocarbons were injected into a He carrier gas stream at several space times, and the conversions were plotted against the space time for each. Before each pule was admitted, the catalyst was reoxidized in an O$_2$–He stream at 823°K. From these conversion/space time data, initial reaction rates were calculated. An activation energy for each was determined from a plot of these rates vs. $1/T$ on a semilog scale. The values of the initial rates, temperatures, and the observed activation energies are given in Table 1. It is apparent that the lin-

ear and cyclic dienes are much more reactive and have lower activation energies than does the propylene.

Tracer Experiments

Two types of isotopic tracer experiments were carried out in the pulse reactor. The first involved pulses of ^{13}C-labeled propylene in the presence of unlabeled [^{12}C]hexadiene and was designed to determine the source of CO$_2$, whether it came from propylene combustion or hexadiene combustion. Standard 2.4 cm^3 (STP) pulses containing 89.2% [^{13}C]propylene (56% enrichment at the C$_3$ position) and 10.8% hexadiene were passed at various space velocities over 15.6 g of the catalyst at 823°K. The mole percentages of ^{13}CO$_2$ and ^{12}CO$_2$ in the effluent stream are plotted versus space time in Fig. 8. Even though the ^{12}C/^{13}C ratio in the reactants was 5.57/1, initially the ^{12}C/^{13}C ratio in the product CO$_2$ was about 25/1, which indicates that the hexadiene is much more rapidly combusted than is the propylene. Since the hexadiene contains twice as many C atoms per molecule as propylene, the relative ratio of hexadiene/propylene combustion is

$$\frac{25}{5.57 \times 2} = 2.22 \qquad (2)$$

when the isotopic enrichment and reaction stoichiometry are taken into account. Simi-

TABLE 1

Microcatalytic Pulse Experiments

Reactant	Temp. (°K)	Initial rate $(dx/d\tau)_0$ $(10^{-3}$ m^3/Kg sec)	E_{act} (Kcal/mole)
Propylene	773	0.00235 ⎫	
Propylene	823	0.00678 ⎬	29.0
Propylene	873	0.02060 ⎭	
1,5-Hexadiene	823	0.138 ⎫	19.0
1,5-Hexadiene	873	0.270 ⎭	
⬡	{823 873}	0.238 0.370	12.5
⬡	{823^a 873^a}	0.416^a 0.566^a	8.7^b

^{a} Calculated by extrapolating data obtained at 723 and 748°K into the proper temperature range.
^{b} Obtained from data at 723 and 748°K.
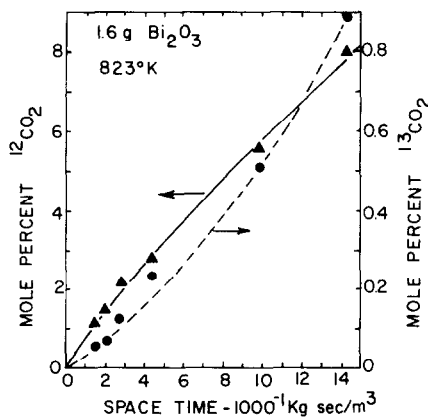
FIG. 8. Distribution of ^{13}C in product CO$_2$ from [^{13}C]propylene/[^{12}C]hexadiene mixture.

lar results were obtained at 873°K where the initial ratio was about 17/1 in the product CO_2.

The second tracer experiment was designed to determine if cleavage of C–H bonds might be involved in the rate-limiting step of the reaction. To shed light on this question, 2.4 cm³ (STP) pulses of a mixture of lightweight (d_0) and heavy (d_5) propylene (d_0 : d_5 = 42.5 : 57.5 mole ratio) were passed over 15.6 g of the catalyst at different temperatures and space velocities. The products were trapped and analyzed for deuterium content. The data shown in Fig. 9 indicate that the lightweight propylene reacts about 1.7 times as rapidly as the deuterated material at 873°K (isotope effect $k_H/k_D = 1.7$) and that there is almost no H–D scrambling among the unreacted propylene molecules. Along the pathway leading to benzene formation, considerable intermolecular H–D scrambling was observed in the benzene product molecules, although the isotopic distribution is far from statistical equilibrium as shown in Fig. 10. However, when pulses of a mixture of d_0 and d_6 benzene were passed over the catalyst under reaction conditions, there was essentially no H–D scrambling among the molecules.

DISCUSSION

Kinetics

An attempt was made to fit the observed rate data to two different types of kinetic models by adjusting the available parameters to give the best fit. The first equation was obtained from a Langmuir–Hinshelwood triple-site, competitive adsorption model

$$-r_{O_2} = k_2(\theta_P)^2(\theta_O)$$

$$= k_2 \frac{(K_P C_P)^2 (K_O C_O)}{(1 + K_P C_P + K_O C_O)^3} \quad (3)$$

which can be integrated to give the linear equation
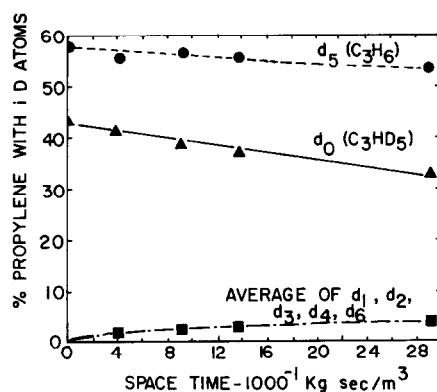
$$m^2 \ln(1 - x) + 3m^2 Ax + \frac{3mA^2}{2}(2x - x^2)$$

FIG. 9. Hydrogen–deuterium scrambling, isotope effects: C_3H_6/C_3HD_5 mixture at 873°K.

$$+ \frac{A^3}{3}(3x - 3x^2 + x^3) = k_2(K_P C_P^\circ)^2 K_O \tau \quad (4)$$

where $m = (1 + K_P C_P^\circ)$ and $A = K_O C_O^\circ$. The fractional surface coverages by propylene and oxygen are expressed as θ_P and θ_O, and the respective adsorption equilibrium constants are K_P and K_O. k_2 is the rate constant for the true surface reaction between adsorbed propylene and adsorbed oxygen. The concentrations of propylene and oxygen entering the catalyst bed are C_P° and C_O°. In this form the oxygen is assumed to be associatively adsorbed.

With the temperature of 823°K selected as a basis point, the constants K_P and K_O
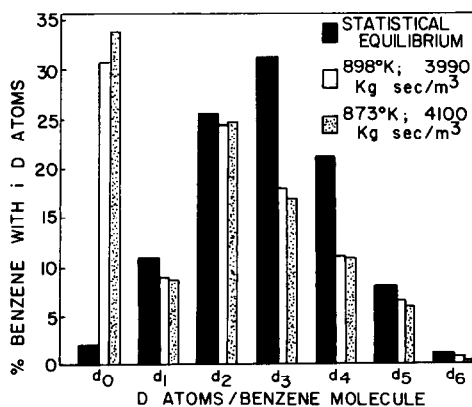
FIG. 10. Hydrogen–deuterium distribution in benzene from C_3H_6/C_3HD_5 mixture at 873°K. Comparison with statistical equilibrium.

can be expressed as

$$K_P = 37.8 \, M^{-1} \exp \frac{-1250}{R} \left(\frac{823 - T}{823 \, T} \right) \quad (5)$$

$$K_O = 34.0 \, M^{-1} \exp \frac{-2500}{R} \left(\frac{823 - T}{823 \, T} \right), \quad (6)$$

where M denotes molar concentration. Using these values, one can plot the left-hand side of Eq. (4) (an explicit function of oxygen converison x) as the ordinate against $(K_P C_P^\circ)^2 K_O \tau$ as the abscissa for each temperature. Figure 11 shows such a plot for two different initial oxygen concentrations at 773°K. The slope of the curve gives k_2 at 773°K. Values of this parameter were similarly obtained at six different temperatures between 748 and 873°K; all the values are shown on the Arrhenius plot in Fig. 12. The plot is reasonably linear and has an activation energy of 21.4 kcal/mole. In spite of this apparent satisfactory correlation of the data, it should be pointed out that this equation is based on associative O_2 adsorption, which is difficult to accept from a mechanistic viewpoint. Rate equations based on dissociative O_2 adsorption were tested and did not fit the data nearly so well as did this associative model.

The same data were also tested according to the Mars–van Krevelen (18) model

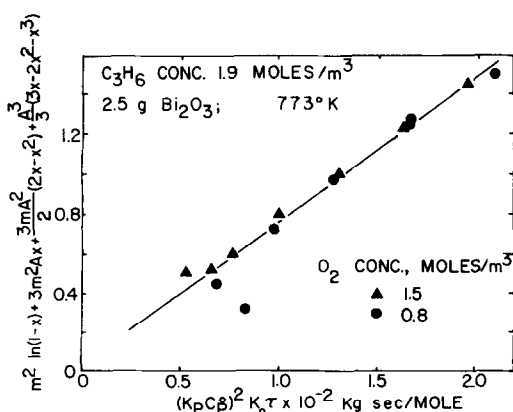$$-\frac{1}{r_{O_2}} = \frac{1}{k_1(C_P)^{1/2}} + \frac{\beta}{k_2(C_O)^{3/2}}, \quad (7)$$
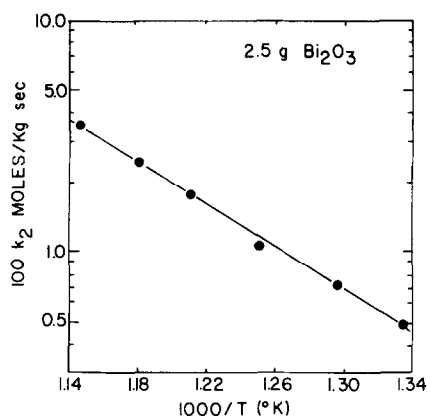

FIG. 12. Arrhenius plot for integrated Langmuir–Hinshelwood model.

where β is the number of oxygen molecules required to oxidize the propylene. Values of k_2 obtained at the same six temperatures used in the Langmuir–Hinshelwood model are shown on an Arrhenius plot in Fig. 13. Note that the data points do not lie on a straight line, although the best least square line through the data gives an "average" activation energy of about 24 kcal/mole. This value is somewhat higher than the value obtained from the initial rate data. For this reason, we favor the Langmuir–Hinshelwood model, though the evidence is not compelling. Even though it correlates the data very well, the Langmuir–Hinshelwood model that gives the best fit has at least two serious shortcomings. First, it assumes associative oxygen adsorption, and secondly the adsorption equilibrium constants increase slightly with temperature instead of decreasing as theory predicts they should.

For correlation purposes, this form of the Langmuir–Hinshelwood equation predicts OXDD reaction rates with oxygen orders varying from -2 to $+1$ as the P_{O_2} is decreased. Thus, it can be used to explain the results reported by Seiyama et al. (25) (negative order in oxygen), Swift et al. (13) (zero order in oxygen), Trimm et al. ($7, 8$) (positive fractional order in oxygen), and

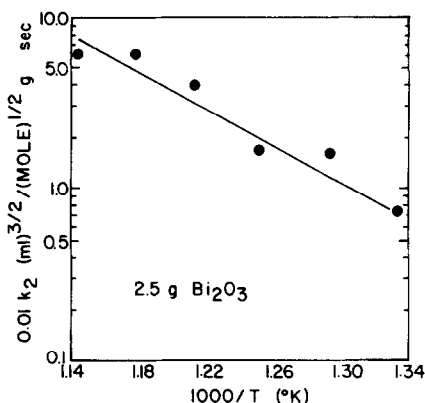FIG. 11. Integrated rate plot. Langmuir–Hinshelwood model.

FIG. 13. Arrhenius plot for integrated Mars–van Krevelen model.

Pashegorova et al. (27) (first order in oxygen).

Oxygen is consumed to form selective products, nonselective products, and for catalyst reoxidation. The site regeneration may be either a dissociative process (8) or an associative process (26) followed by disproportionation of S–O_2 and S-(vacant) to form two S–O species. The path to total combustion products may involve either (or both) chemisorbed or lattice oxygen (28). Since our microreactor results showed that 1,5-hexadiene could be oxidized to CO_2 in the absence of gaseous O_2, lattice oxygen must clearly be involved. The path to selective products is generally thought to involve lattice oxygen, which is zero order in oxygen, although some researchers (29) have postulated a hydrocarbon peroxide ion mechanism for the selective oxidation of propylene, a related reaction. The summation of all these contributions indicates that the oxygen order may vary between zero and first order, depending on which is rate controlling. Our rate data (Fig. 3) support this conclusion, although it is not possible to assign relative contributions to each of these selective, nonselective, and site-regeneration processes. In short, our rate equation does not rule out any mechanisms that have been proposed for reoxidation of the catalyst.

Reaction Pathways

It is apparent from the data shown in Fig. 8 that the CO_2 is formed initially from *both* propylene and hexadiene. The fact that the $^{12}C/^{13}C$ ratio in the products exceeds that in the reactants means the unlabeled diene is more easily combusted than the labeled propylene. This is true even though the partial pressure of the propylene is almost an order of magnitude larger than the partial pressure of the diene. Under these conditions, the rate of diene combustion is about double that of the propylene.

Since the initial ratio of $^{12}C/^{13}C$ is not infinity at infinite space velocity (i.e., the ^{13}C curve in Fig. 8 does not have an initial slope of zero), the pathway(s) leading to CO_2 formation do not pass *exclusively* through the hexadiene.

Our observed activation energy (29.0 kcal/mole) for propylene consumption in absence of gaseous O_2 compares favorably with those reported by Swift et al. (13) (27.5 kcal/mole) and by Massoth and Scarpiello (22) (27.0 kcal/mole) for the kinetic-controlled reaction of propylene over Bi_2O_3. When gaseous O_2 was present, our observed activation energy (22 kcal/mole) may have been disguised by diffusional limitations, as indicated by the changes in selectivity with particle size (Fig. 6).

These observations lead us to suggest the following reaction scheme, shown only for the hydrocarbon species and CO_2.
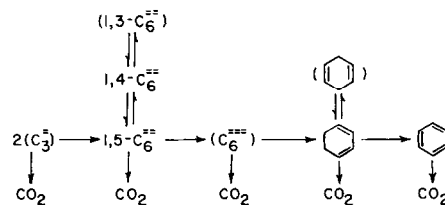

The species shown in parentheses were not actually observed. Dienes are indicated by the symbol $C_6^{==}$; trienes are $C_6^{===}$. According to this scheme two propylene molecules are coupled to form the 1,5-hexadiene. As seen in Fig. 7, some of the 1,4-hexadiene isomer was also observed,

although its amount was almost negligible. When pulses of the 1,5-hexadiene were passed through the reactor, some cyclization to 1,3-cyclohexadiene was observed, along with benzene and CO_2. To account for this, we assume that the diene is further oxidatively dehydrogenated to the *triene* which cyclizes to 1,3-cyclohexadiene, an observed product. This step is very likely thermal, not catalytic, as the triene has been shown to cyclize rapidly without a catalyst at temperatures as low as 473°K (*19*). That the triene was not an observed product is not surprising since it is such a reactive species under these conditions. Finally, the cyclohexadiene can further dehydrogenate (perhaps oxidatively) to yield the final product benzene. Any of these species may well be oxidized to CO_2 along the way, although the diene seems to be the most reactive in this regard.

Since all the microreactor pulse tests were conducted in the absence of gaseous O_2, lattice oxygen is the primary oxidant after the first pulse has "cleaned" the surface of chemisorbed oxygen. In a previous paper, we (*23*) have offered evidence (based on changes in electrical properties of the solid) that most of the surface sorbed oxygen is removed from Bi_2O_3 by brief contact with propylene. The product distributions obtained from a series of propylene pulses also show the effect of the sorbed oxygen. The first pulse gave high conversion (80%) and low selectivity, whereas subsequent pulses showed only about 20% conversion and much higher selectivities to C_6 compounds.

Rate-Limiting Step

The large $k_H/k_D \sim 1.7$ primary kinetic isotope effect at 873°K (Fig. 9) clearly shows that cleavage of C–H bonds is involved in the rate-limiting step of the reaction. Most likely a hydrogen atom is lost from the C-3 position in the propylene to form a symmetric allylic radical

$$H_2C{=}\overset{\displaystyle H}{\underset{\displaystyle |}{C}}{=}CH_2,$$
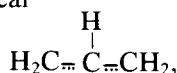
and two of these species then are coupled to form 1,5-hexadiene. Presumably the two H atoms that are extracted in the rate-limiting step form surface hydroxyl groups by reaction with adsorbed O atoms, as has been shown to occur in other oxidative dehydrogenation reactions to form diolefins from monoolefins (*20*). The fact that two C–H bonds must be broken may account for the extremely large isotope effect at this high temperature. Thus having identified the slow step in the reaction, it should now be possible to improve the catalytic activity by incorporating additional C–H bond breaking ability into the catalyst formulation. The large kinetic isotope effect is in general agreement with results obtained by Grasselli *et al.* (*21*) during ammoxidation over bismuth molybdates.

Isotope Scrambling

Because of fragmentation problems, it was impossible to measure the parent peaks of the 1,5-hexadiene directly in the mass spectrometer. For that reason the deuterium isotopic composition could not be determined accurately. However, it was possible to measure parent peaks of the benzene, and this molecule was used to determine the degree of isotopic scrambling in the products.

It is apparent from Fig. 10 that the isotopic distribution in the benzene is quite different from that predicted by statistical equilibrium. These data can be partially explained by considering the coupling of two symmetric allylic species formed on the surface from the labeled and unlabeled propylene molecules. Because of its ease of formation relative to the deuterated species, the unlabeled allylic radical will be the dominant surface species and will then react more rapidly to form the products than does its deuterated analog. This relative activity is indicated by the weight of lines in the following reaction scheme involving coupling of two allylic radicals.
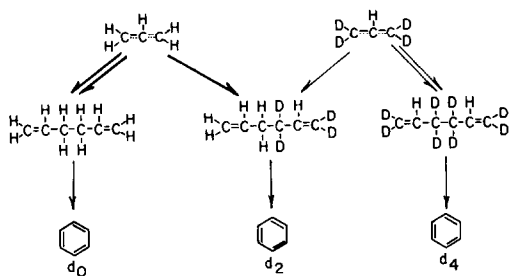
The relative abundance of labeled benzenes should then follow the order $d_0 > d_2 > d_4$, and there should be no species with an odd number of D atoms if the scheme were strictly followed. This is indeed the order followed by the abundances shown in Fig. 10, although the d_3 species being greater than d_4 indicates that there is considerable (although not nearly statistical) scrambling of H and D atoms among the molecules. This scrambling must occur *before* benzene formation, for mixtures of benzene d_0 and d_6 passed over the catalyst under the same reaction conditions showed almost no isotopic mixing.

CONCLUSIONS

Bismuth oxide is a moderately selective catalyst for making 1,5-hexadiene (and benzene) from propylene. The major side product is CO_2 which is formed via series–parallel reaction pathways involving the propylene reactant and all other hydrocarbon products. 1,3-Cyclohexadiene is an intermediate en route to benzene, presumably formed by the thermal cyclization of hexatriene. A large primary kinetic isotope effect shows that the rate-limiting step of the reaction is removal of an H atom from the propylene. We propose that symmetric allylic radicals are formed on the surface and that two of these are then coupled to form 1,5-hexadiene. Some isotopic scrambling occurs, but the extent of this scrambling is insufficient to obscure the isotopic origin of the product molecules. The kinetic data can be fit satisfactorily to a triple-site Langmuir–Hinshelwood rate model where the surface reaction has an activation energy of 22 kcal/mole (92.1 kJ/mole); how-

ever, this model involves some untenable assumptions. Changes in the particle size do not alter the overall activity, although the selectivity for the C_6 products is decreased relative to CO_2 as the particle size is increased.

REFERENCES

1. Friedli, H. R., U.S. Patent No. 3,769,361.
2. Friedli, H. R., U.S. Patent No. 3,494,972.
3. Morre, W. P., U.S. Patent No. 3,435,089.
4. D'Alessandro, A. F., U.S. Patent No. 3,830,866.
5. Friedli, H. R., Hart, P. J., and Vrieland, G. E., Symposium on Catalytic Oxidation of Hydrocarbons, ACS New York Meeting, 1969.
6. Hart, P. J., and Friedli, H. R., *J. Chem. Commun.* **11**, 621 (1960).
7. Trimm, D. L., and Doerr, L. A., *J. Catal.* **23**, 49 (1971).
8. Trimm, D. L., and Doerr, L. A., *J. Catal.* **26**, 1 (1972).
9. Seiyama, T., Egashira, M., Sakamoto, T., and Aso, I., *J Catal.* **24**, 76 (1976).
10. Schultz, R. G., and Wildi, J. M., *J. Catal.* **6**, 385 (1966).
11. Schultz, R. G., Engelbrecht, R. M., Moore, R. N., and Wolford, L. T., *J. Catal.* **6**, 419 (1966).
12. Schultz, R. G., *J. Catal.* **7**, 286 (1967).
13. Swift, H. E., Bozik, J. E., and Ondrey, J. A., *J. Catal.* **21**, 212 (1971).
14. Solymosi, F., and Kiss, J., *J. Catal.* **41**, 202 (1976).
15. Solymosi, F., and Bozsó, F., Fifth International Congress on Catalysis, London, p. 365, 1976.
16. Mamedov, E. A., Gamid-Zade, E. G., and Rizaev, R. G., *React. Kinet. Catal. Lett.* **8**, 227 (1978).
17. Greene, P. A., et al., U.S. Patent No. 3,494,956.
18. Mars, P., and van Krevelen, D. W., *Spec. Suppl. Chem. Eng. Sci.* **3**, 41 (1954).
19. Lewis, E. K., and Steiner, H., *J. Chem. Soc.* 3080 (1964).
20. Gibson, M. A., and Hightower, J. W., *J. Catal.* **41**, 420 (1976).
21. Burrington, J. D., Kartisek, C. T., and Grasselli, R. K., *J. Catal.* **63**, 235 (1980).
22. Massoth, F. E., and Scarpiello, D. A., *J. Catal.* **21**, 225 (1971).
23. White, M. G., and Hightower, J. W., *AIChE J.* **27**, 545 (1981).
24. Mamedov, E. A., *Russ. Chem. Rev.* **50**, 29 (1981).

25. Seiyama, T., Uda, T., Mochida, I., and Egashira, M., *J. Catal.* **34,** 29 (1974).
26. Mamedov, E. A., Gamid-zade, E. G., Agaev, F. M., and Rizaev, R. G., *Kinet. Katal.* **20,** 410 (1979).
27. Pashegorova, V. S., Kaliberdo, L. M., and Lebedeva, G. G., *Neftekhimiya* **16,** 840 (1976).
28. Gamid-zade, E. G., Mamedov, E. A., and Rizaev, R. G., *Kinet. Katal.* **20,** 405 (1979).
29. Margolis, L. Ya., *Adv. Catal.* **14,** 429 (1963).